Synaptotagmin-1 Utilizes Membrane Bending and SNARE Binding to Drive Fusion Pore Expansion

**Kara L. Lynch,* Roy R.L. Gerona,* Dana M. Kielar,* Sascha Martens,†
Harvey T. McMahon,† and Thomas F.J. Martin***

*Department of Biochemistry, University of Wisconsin, Madison, WI 53706; and †Medical Research Council
Laboratory of Molecular Biology, Cambridge CB2 2QH, United Kingom

In regulated vesicle exocytosis, SNARE protein complexes drive membrane fusion to connect the vesicle lumen with the extracellular space. The triggering of fusion pore formation by Ca^{2+} is mediated by specific isoforms of synaptotagmin (Syt), which employ both SNARE complex and membrane binding. Ca^{2+} also promotes fusion pore expansion and Syts have been implicated in this process but the mechanisms involved are unclear. We determined the role of Ca^{2+}-dependent Syt-effector interactions in fusion pore expansion by expressing Syt-1 mutants selectively altered in Ca^{2+}-dependent SNARE binding or in Ca^{2+}-dependent membrane insertion in PC12 cells that lack vesicle Syts. The release of different-sized fluorescent peptide-EGFP vesicle cargo or the vesicle capture of different-sized external fluorescent probes was used to assess the extent of fusion pore dilation. We found that PC12 cells expressing partial loss-of-function Syt-1 mutants impaired in Ca^{2+}-dependent SNARE binding exhibited reduced fusion pore opening probabilities and reduced fusion pore expansion. Cells with gain-of-function Syt-1 mutants for Ca^{2+}-dependent membrane insertion exhibited normal fusion pore opening probabilities but the fusion pores dilated extensively. The results indicate that Syt-1 uses both Ca^{2+}-dependent membrane insertion and SNARE binding to drive fusion pore expansion.

INTRODUCTION

Neurotransmitter and peptide hormone secretion is mediated by the Ca^{2+}-dependent exocytosis of vesicles at the plasma membrane. Vesicle fusion proceeds through membrane intermediates of stalk formation, fusion pore opening, and fusion pore expansion (Lindau and Alvarez de Toledo, 2003). In classical modes of vesicle exocytosis, fusion pores expand to the point where the vesicle membrane flattens on the plasma membrane (full fusion), leading to complete luminal contents release (full release). However, vesicle exocytosis can utilize alternative modes in which the fusion pore either abruptly closes (kiss-and-run) or in which the fusion pore dilates but subsequently recloses (cavicapture; Henkel and Almers, 1996). These transient modes of vesicle exocytosis lead to the partial release of luminal contents depending on the size and diffusibility of the cargo (Alvarez de Toledo et al., 1993; Barg et al., 2002; Taraska et al., 2003). Ca^{2+} levels regulate fusion pore expansion as well as fusion pore formation (Fernandez-Chacon and Alvarez de Toledo, 1995; Hartmann and Lindau, 1995; Wang et al., 2006), but the mechanisms underlying fusion pore expansion, which is the more energetically demanding step, are poorly understood (Cohen and Melikyan, 2004).

A Ca^{2+}-dependent fusion machinery mediates the triggered formation of fusion pores. Three SNARE proteins (VAMP-2 on the vesicle with SNAP25 and syntaxin-1 on the plasma membrane) form *trans* complexes that promote close

membrane apposition and membrane fusion (Weber et al., 1998). Members of the synaptotagmin (Syt) protein family that localize to vesicles function as Ca^{2+} sensors that couple Ca^{2+} rises to vesicle exocytosis (Chapman, 2002; Sudhof, 2004; Rizo et al., 2006). Syt-1 is the best understood isoform and functions as a synaptic vesicle Ca^{2+} sensor for the rapid synchronous release (Geppert et al., 1994) but not for the slow asynchronous release of neurotransmitter (Sun et al., 2007) in hippocampal neurons. Syt-2 and -9 likely play similar roles at other synapses (Xu et al., 2007). Syt-1 and -9 also cofunction as essential Ca^{2+} sensors for dense-core vesicle exocytosis in PC12 cells (Lynch and Martin, 2007), whereas Syt-1 and -7 contribute to Ca^{2+}-triggered dense-core vesicle exocytosis in chromaffin cells (Schonn et al., 2008). Syts-1, -7, and -9 have also been reported to mediate Ca^{2+}-triggered dense-core vesicle exocytosis in pancreatic β-cells (Iezzi et al., 2005; Xiong et al., 2006; Gustavsson et al., 2008). The function of most other members of the 17 member Syt family remains to be clarified (Craxton, 2007).

Syts contain two cytoplasmic C2 domains, C2A and C2B, each of which are eight-stranded β-sandwiches connected by three flexible loops. The Ca^{2+}-binding Syt isoforms such as Syt-1 contain conserved Ca^{2+}-binding aspartate residues in loops 1 and 3 of the C2 domains. Ca^{2+} binding imparts a positive electrostatic potential to the C2 domain surface that enables the binding of Syt-1 to its effectors by neutralizing acidic residues in the Ca^{2+}-binding loops (Rizo and Sudhof, 1998; Bai and Chapman, 2004). The two major effectors for Syt-1 are acidic residues on the surface of SNARE complexes and anionic phospholipids in the plasma membrane.

Ca^{2+} binding to Syt-1 promotes the binding of tandem C2 domains to syntaxin-1 and SNAP25 as well as to SNARE protein complexes (Davis et al., 1999; Gerona et al., 2000; Earles et al., 2001; Bai et al., 2004). Ca^{2+}-dependent Syt-1–

SNARE interactions are mediated in part by acidic residues in the SNAP25 C-terminus binding to basic residues in Syt-1 C2A loop 2 (Zhang *et al.*, 2002; Lynch *et al.*, 2007). Syt-1 mutations that eliminate Ca^{2+}-dependent SNARE binding abrogate Ca^{2+}-triggered dense-core vesicle exocytosis in PC12 cells (Lynch *et al.*, 2007), whereas mutations that enhance SNARE binding facilitate Ca^{2+}-triggered synaptic vesicle exocytosis in neurons (Pang *et al.*, 2006). The Ca^{2+} regulation of liposome fusion mediated by Syt-1 requires Syt-1–SNARE interactions (Bhalla *et al.*, 2006). These findings indicate an essential role for SNARE binding in determining Ca^{2+}-dependent vesicle fusion probabilities.

Anionic phospholipids are a second important Syt-1 effector for Ca^{2+}-triggered vesicle fusion. The Ca^{2+}-dependent switch in electrostatic surface potential of Syt-1 promotes interactions with acidic phospholipid headgroups (Zhang *et al.*, 1998) and results in the partial insertion of hydrophobic residues at the tips of C2 domain loops 1 and 3 (M173/F234/V304/I367) into the lipid bilayer (Bai *et al.*, 2002; Herrick *et al.*, 2006). Bilayer penetration by the tandem C2 domains induces positive curvature in membranes, which may lower the activation energy required for fusion (Martens *et al.*, 2007). Syt-1 mutants with alanines at the tips of loops 1 and 3 fail to induce membrane curvature or to confer Ca^{2+} regulation on SNARE-mediated liposome fusion (Martens *et al.*, 2007). Conversely, tryptophan replacements enhance Ca^{2+}-dependent lipid binding and increase the Ca^{2+}-dependent probability of synaptic vesicle fusion in neurons (Rhee *et al.*, 2005).

Beyond their role in determining Ca^{2+}-dependent vesicle fusion probabilities, Syts also regulate fusion pore expansion (Jackson and Chapman, 2006). Syt-1 overexpression increases the lifespan of dense-core vesicle fusion pores inferred from measurements of a prespike foot (PSF) in amperometric recordings of catecholamine release from PC12 cells (Wang *et al.*, 2001). These overexpression effects of Syt-1 require Ca^{2+} binding residues and proper inter-C2 domain spacing (Wang *et al.*, 2003, 2006; Bai *et al.*, 2004). It remains to be determined whether endogenous Syt-1 regulates dense-core vesicle fusion pore expansion and if so, whether Syt-1 utilizes membrane binding and curvature induction, or interactions with SNAREs, or both. To address these issues, we introduced Syt-1 with mutations that selectively alter Ca^{2+}-dependent membrane insertion or SNARE interactions into PC12 cells that lack vesicle Syts (Lynch and Martin, 2007). We used fluorescent probes of distinct sizes to assess the extent of fusion pore dilation. The data indicate that reduced Syt-1–SNARE interactions markedly decrease normal fusion pore dilation, whereas increased Syt-1-membrane insertion drives extensive fusion pore opening. We conclude that Syt-1 uses both Ca^{2+}-dependent membrane bending and SNARE binding to drive fusion pore expansion.

MATERIALS AND METHODS

Antibodies and DNA Constructs

Antibodies used were Syt-1 monoclonal (clone 604.1; Synaptic Systems, Göttingen, Germany), Syt-1 N-terminal polyclonal (Sigma-Aldrich, St. Louis, MO) and a Syt-1 polyclonal antibody generated using a Syt-1 C2AB fusion protein. The plasmid encoding atrial natriuretic factor (ANF)-enhanced green fluorescent protein (EGFP) was provided by E. Levitan (University of Pittsburgh School of Medicine, Pittsburgh, PA) and the plasmid encoding brain-derived neurotrophic factor (BDNF)-EGFP by V. Lessmann (Johannes Gutenberg Universität, Mainz, Germany). Oligonucleotides encoding Syt-1/9 shRNAs (Lynch and Martin, 2007) were ligated into pSHAG-1 vector (Paddison *et al.*, 2002) via BamHI and BseRI sites. The open reading frame of Syt-1 was reverse-transcribed and PCR-amplified from rat PC12 cells and ligated into pcDNA3.1 (Invitrogen, Carlsbad, CA). The QuickChange Site-Directed Mutagenesis method (Stratagene, La Jolla, CA) was used to generate the Syt-1 silent mutant, pcDNA3-syt I sm (Lynch and Martin, 2007), and the R199A/K200A, M173A/F234A/V304A/I367A and M173W/F234W/V304W/I367W mutations were introduced into the pcDNA3-syt I sm construct.

Fusion Proteins and Liposome-binding Assays

Constructs encoding C2AB fusion proteins for production in *E. coli* corresponding to Syt-1^{RK}, Syt-1^{4A}, and Syt-1^{4W} have been described (Lynch *et al.*, 2007; Martens *et al.*, 2007). The preparation of liposomes containing ~80 copies of SNAP25/syntaxin-1 in 85% 1,2-dioleoyl-*sn*-glycero-phosphatidylcholine (DOPC) and 15% 1,2-dioleoyl-*sn*-glycero-phosphatidylserine (DOPS) from Avanti Polar Lipids (Alabaster, AL) has been described (Weber *et al.*, 1998; Lynch *et al.*, 2007). Protein-free liposomes of indicated composition were similarly prepared by detergent dialysis. Binding studies were conducted with 10 μM wild-type or mutant C2AB incubated with ~1.25 mM liposomes in 25 mM HEPES, pH 7.2, 100 mM KCl, and 0.2 mM EGTA plus $CaCl_2$ for 30 min at room temperature. Free ionic Ca^{2+} concentrations were calculated with the CHELATOR program (Schoenmakers *et al.*, 1992). Bound C2AB was isolated by buoyant density flotation on Accudenz gradients (40, 30, and 0% vol/vol) by centrifugation at 190,000 $\times$ *g* at 4°C for 4 h (Lynch *et al.*, 2007). Material at the 0/30% interface was collected, analyzed by SDS gel electrophoresis, and stained with colloidal Commassie Blue for quantification with a Molecular Dynamics SI Densitometer using Image Quant software (Sunnyvale, CA).

Cell Culture, Transfection, Immunoblot Analysis, and Immunocytochemistry

PC12 cells were cultured in DMEM supplemented with 5% horse serum and 5% calf serum. Transfection was conducted by electroporation using an Electroporator II (Invitrogen). The Syt-1/9-null PC12 cell line was isolated as described previously (Lynch and Martin, 2007). Syt-1 and -9 are the major Syt isoforms on dense-core vesicles in PC12 cells and their elimination by short hairpin RNA (shRNA) knock down results in a full loss of Ca^{2+}-triggered vesicle exocytosis (Lynch and Martin, 2007). Although Syt-7 overexpression affects Ca^{2+}-dependent vesicle exocytosis in PC12 cells (Fukuda *et al.*, 2004; Wang *et al.*, 2005), Syt-7 is present endogenously at very low levels (37- and 21-fold less than Syt-1 and -9, respectively; Tucker *et al.*, 2003) and contributes very little to Ca^{2+}-triggered dense-core vesicle exocytosis based on shRNA knock down (Supplemental Figure S1).

Protein expression levels were determined from total cell lysates prepared in 1 mM PMSF and 1% Triton X-100 and clarified by centrifugation at 16,000 $\times$ *g* for 5 min. Twenty micrograms of total protein determined by bicinchoninic acid (BCA) assay (Pierce Chemical, Rockford, IL) was loaded per lane for gel electrophoresis. Immunoblot analysis was conducted by standard methods. For immunocytochemistry, cells were plated on poly-DL-lysine- and collagen-coated coverslips. Cells were washed with PBS, fixed with 4% formaldehyde (wt/vol), permeabilized with 0.3% Triton X-100 in PBS, and blocked in 10% FBS in PBS. Primary and secondary antibodies were diluted in FBS blocking solution. Coverslips were mounted on slides with Mowiol 4-88 Reagent (Calbiochem, EMD Chemicals, La Jolla, CA), and cells were imaged on a C1 laser scanning confocal microscope with a 60× oil immersion objective with NA 1.4 (Nikon Instruments, Melville, NY).

Exocytosis and Dextran Uptake Assays

Cells were transiently transfected and plated on 35-mm glass-bottom dishes (MatTek, Ashland, MA) coated with poly-DL-lysine and collagen. After 48 h, cells were imaged on a Nikon TIRF microscope evanescent wave imaging system on a TE2000-U inverted microscope (Nikon Instruments) with an Apo TIRF 100×, NA 1.45 objective lens. EGFP fluorescence was excited with the 488-nm laser line of an argon ion laser. Calibration studies indicated that the exponential evanescent field of the total internal reflection fluorescence (TIRF) optical system had a penetration depth (1/e) of ~80 nm in 1.37 refractive index medium equivalent to cytosol. Cells were imaged in basal media (15 mM HEPES, pH 7.4, 145 mM NaCl, 5.6 mM KCl, 2.2 mM $CaCl_2$, 0.5 mM $MgCl_2$, 5.6 mM glucose, 0.5 mM ascorbic acid, and 0.1% BSA) or depolarization medium (same as basal medium with 95 mM NaCl and 56 mM KCl). Images were acquired at 75- or 250-ms intervals with a CoolSNAP-ES digital monochrome CCD camera system (Photometrics, Tucson, AZ) controlled by Metamorph software (Molecular Devices, Downingtown, PA). Vesicles were identified manually in sequence stacks of images, and their fluorescence determined as circular regions of interest using Metamorph software. All fluorescence values were corrected by background subtraction using circular regions of interest in regions of the image lacking vesicles.

For dextran dye uptake, transfected cells expressing BDNF-EGFP were incubated for 5 min at room temperature in depolarization medium containing Texas red dextrans (50 μM) from Molecular Probes (Invitrogen). Cells were washed with PBS and imaged on a Nikon C1 laser scanning confocal microscope with a 100× oil immersion objective with NA 1.4. The number of BDNF-EGFP–containing vesicles that captured 10-, 40-, and 70-kDa Texas red dextrans was determined from a bottom confocal section of the cell. The average number of exocytic events occurring in 5-min stimulations was

determined by TIRF microscopy as described above and was used to normalize the dextran capture results.

Structures for ANF-EGFP and BDNF-EGFP are not available. We estimated a molecular diameter for an ANF-EGFP monomer of ~6 nm and for a BDNF-EGFP dimer of ~8 nm based on empirical plots of Stokes radius versus molecular mass, assuming that these are globular proteins. Molecular diameters for Texas red dextrans were estimated with the equation: r (in nm) = 0.033 (MW in Da)$^{0.463}$ (Granath and Kvist, 1967).

RESULTS

Syt-1 Mutations Selectively Alter Ca²⁺-dependent SNARE or Membrane Interactions In Vitro

Our strategy was to examine vesicle fusion pore dilation in PC12 cells that harbored mutant versions of Syt-1 that are selectively altered in Ca^{2+}-dependent SNARE or Ca^{2+}-dependent membrane interactions. To selectively alter Syt-1–membrane interactions, we used Syt-1 mutants with tryptophan (called Syt-1^{4W}) or alanine (called Syt-1^{4A}) substitutions for the hydrophobic residues (M173, F234, V304, and I367) at the tips of loops 1 and 3 of the C2 domains (Martens *et al.*, 2007). A Syt-1 C2AB protein with 4W mutations exhibited enhanced Ca^{2+}-dependent PC/PS liposome binding, whereas binding to PC/PS liposomes by C2AB with 4A mutations was reduced (Figure 1B) as previously reported (Martens *et al.*, 2007). Similarly, Ca^{2+}-dependent binding of C2AB to PC/PIP$_2$ liposomes was enhanced by 4W mutations and reduced by 4A mutations (Figure 1C).
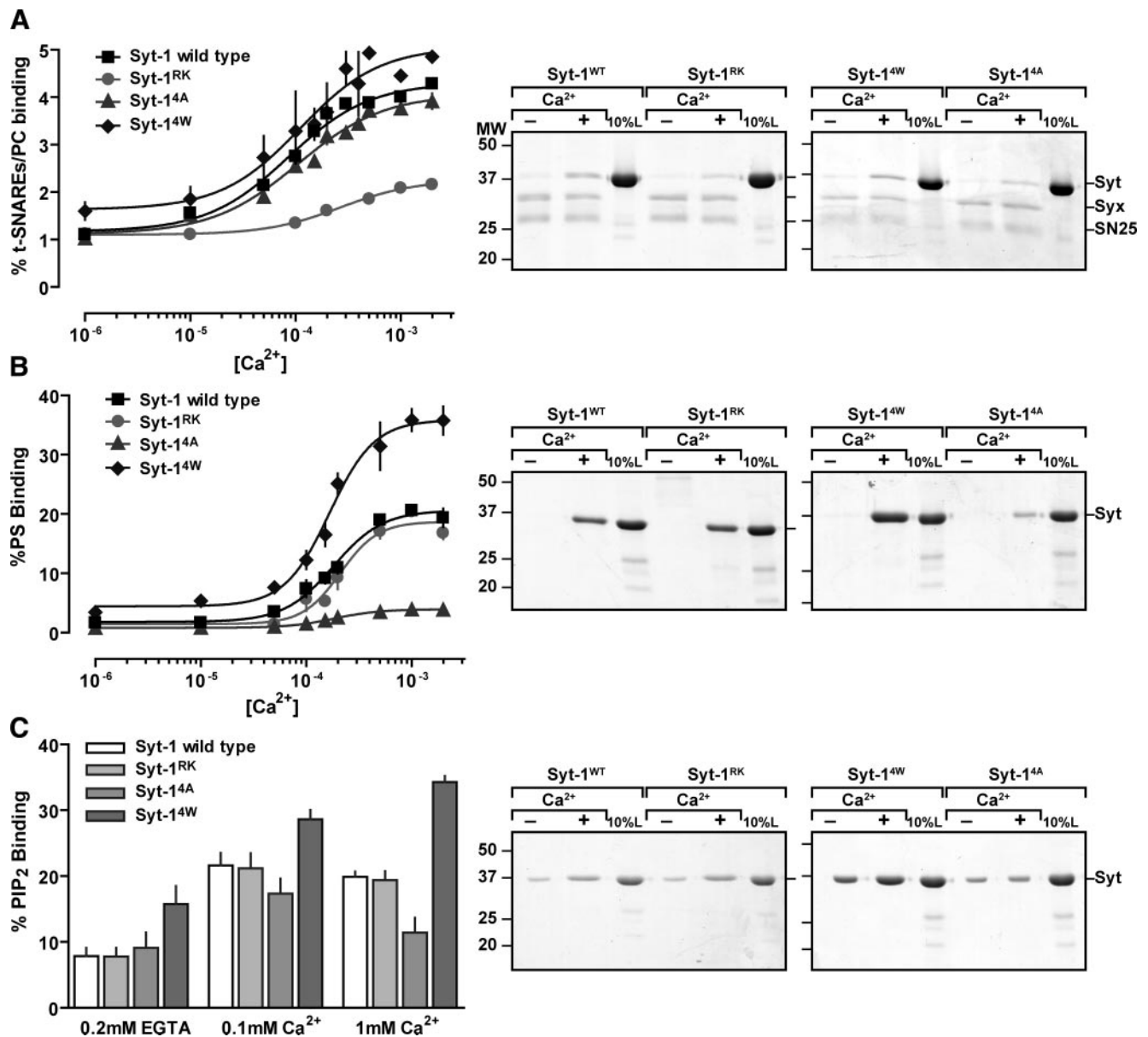
Figure 1. Syt-1 mutants exhibit selective alterations in either Ca^{2+}-dependent SNARE interactions or membrane insertion. Syt-1 C2AB fusion proteins, either wild-type or the indicated mutant versions (Syt-1^{RK}, -1^{4A}, -1^{4W}), were incubated at 10 μM with the indicated Ca^{2+} concentrations with (A) PC liposomes containing syntaxin-1 and SNAP25, (B) protein-free PC/PS (85:15) liposomes, or (C) protein-free PC/PIP$_2$ (95:5) liposomes. Liposome-bound C2AB was isolated from Accudenz gradients and analyzed by SDS-PAGE and Coomassie staining to determine % bound C2AB, indicated as means ($\pm$SE, n = 3). Representative gels from Syt-1 C2AB binding studies conducted with EGTA ($-$) or 1 mM Ca^{2+} ($+$) are shown in the right-hand panels comparing 25% of bound samples with 10% of input Syt-1 C2AB.

Syt-1^{4A} C2AB also fails to promote membrane curvature on liposomes in the presence of Ca^{2+}, whereas Syt-1^{4W} C2AB causes extensive liposome tubulation (Martens *et al.,* 2007). By contrast, the Ca^{2+}-dependent binding of either C2AB with 4A mutations or C2AB with 4W mutations to SNARE-containing PC liposomes was indistinguishable from binding by wild-type C2AB (Figure 1A). The results indicated that Syt-1^{4A} and -1^{4W} are selective loss-of-function and gain-of-function mutants, respectively, for Ca^{2+}-dependent membrane interactions and curvature induction, but they retain wild-type Ca^{2+}-dependent SNARE-binding properties.

To selectively reduce Syt-1–SNARE interactions, we used previously characterized Syt-1 mutants (Lynch *et al.,* 2007). Syt-1 C2A loop 2 mutations (R199A/K200A) combined with C2B loop 1 mutations (K297A/K301A; called Syt-1$^{RK/KK}$) completely abolish Ca^{2+}-dependent binding to SNARE complexes in vitro and eliminate Ca^{2+}-triggered vesicle exocytosis in cells (Lynch *et al.,* 2007). To reduce, but not eliminate, Ca^{2+}-triggered vesicle exocytosis, we used a partial loss-of-function Syt-1 mutant (called Syt-1^{RK}) that contains the C2A loop 2 mutations (R199A/K200A). A C2AB fusion protein with RK mutations exhibited strongly attenuated Ca^{2+}-dependent binding to SNARE-containing PC liposomes in vitro (Figure 1A). By contrast, C2AB with RK mutations exhibited full wild-type Ca^{2+}-dependent binding to PC/PS (85:15) liposomes (Figure 1B) or to PC/PIP$_2$ (95:5) liposomes (Figure 1C). The results confirmed that Syt-1^{RK} is a partial loss-of-function mutant that is selectively altered in Ca^{2+}-dependent SNARE binding but not Ca^{2+}-dependent membrane interactions (Lynch *et al.,* 2007).

Syt Effector Interactions Regulate Fusion Pore Opening

To determine the function of Syt-1 mutant proteins, we expressed them in substitution for endogenous vesicle Syts in PC12 cells. shRNA-expressing PC12 cell lines that lack vesicle Syts (Syt-1 and -9) do not exhibit Ca^{2+}-triggered vesicle exocytosis but can be fully rescued by expression of Syt-1 or -9 constructs with silent mutations that by-pass the shRNA targeting (Lynch and Martin, 2007). Thus, we tested Syt-1 rescue constructs that encode Syt-1^{RK}, -1^{4A}, and -1^{4W}. Wild-type and mutant Syts were expressed at levels comparable to those in wild-type PC12 cells and were targeted to dense-core vesicles in the Syt-1/9-null cells (Supplemental Figure S2; Lynch *et al.,* 2007).

Our initial studies of dense-core vesicle exocytosis used ANF-EGFP cargo, which was similarly expressed and packaged into the dense-core vesicles in wild-type and Syt mutant-expressing cells (Supplemental Figure S3A). Incubation in depolarizing high K$^+$ buffer was used to promote Ca^{2+} influx and trigger dense-core vesicle exocytosis. Exocytic events were detected as fluorescence changes in ANF-EGFP by TIRF microscopy (Lynch *et al.,* 2007; Lynch and Martin, 2007). The time course of averaged cumulative fusion events over the first 60 s of incubation in high K$^+$ buffer revealed that wild-type PC12 cells exhibited 17.0 ± 1.4 (±SE, n = 20) events within the adherent cell footprint (Figure 2A). Syt-1/9-null cells exhibited only 0.4 ± 0.2 (±SE, n = 20) events but Syt-1 expression in Syt-1/9-null cells fully restored Ca^{2+}-triggered vesicle exocytosis with an average of 15.2 ± 1.5 (±SE, n = 20) fusion events (Figure 2A), confirming previous results (Lynch *et al.,* 2007). Expression of Syt-1^{4A}, which is loss-of-function for promoting membrane curvature, largely failed to restore Ca^{2+}-triggered vesicle exocytosis (2.2 ± 0.1 fusion events, ±SE, n = 18; Figure 2A). By contrast, expression of Syt-1^{4W}, which is gain-of-function for promoting membrane curvature, fully rescued Ca^{2+}-triggered exocytosis (15.6 ± 0.3 fusion events, ±SE, n = 10; Figure 2A). Expression of Syt-1^{RK},
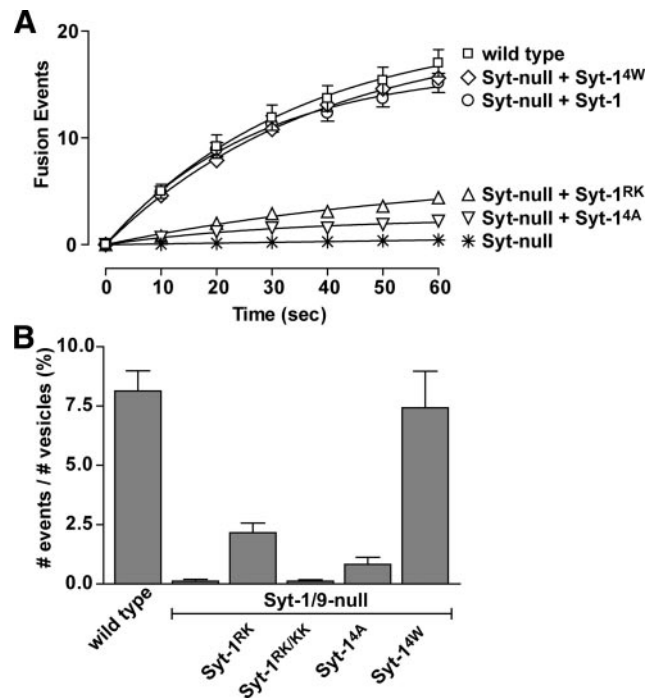
Figure 2. Ca^{2+}-dependent SNARE binding and membrane insertion by Syt-1 regulate fusion pore opening probabilities. (A) Cells expressing ANF-EGFP were stimulated with depolarization medium and TIRF images were acquired at 0.25-s intervals. Fusion events were counted as a flash of vesicle fluorescence in adherent cell footprints, and the cumulative sum of fusion events in 10-s intervals was determined. The sums of the average number of fusion events per cell over time (mean value ±SE) for wild-type cells (n = 20), Syt-null cells (n = 20), Syt-null cells expressing Syt-1^{RK} (n = 20), Syt-null cells expressing Syt-1$^{RK/KK}$ (n = 10), Syt-null cells expressing Syt-1^{4A} (n = 18), and Syt-null cells expressing Syt-1^{4W} (n = 10) were plotted. Syt-null corresponds to cells down regulated for vesicle Syt-1 and -9. (B) Fusion probabilities after stimulation were calculated as the number of release events in 60 s divided by the number of plasma membrane-proximal vesicles (mean value ±SE) for each cell type.

which is partial loss-of-function for SNARE binding, only partially restored Ca^{2+}-triggered vesicle exocytosis (4.4 ± 1.1 fusion events, ±SE, n = 10; Figure 2A) similar to previous results (Lynch *et al.,* 2007).

Vesicle fusion probabilities after stimulation were calculated as the percent of plasma membrane-proximal resident vesicles in the evanescent field that exhibited exocytosis in 60 s (Figure 2B). The number of plasma membrane-proximal resident vesicles was the same for cells expressing wild-type or mutant Syts (Supplemental Figure S3C) and most (≥75%) of the exocytic events occurred from the plasma membrane–resident vesicles (not shown). Vesicle release probabilities were close to zero in cells lacking vesicle Syts (Figure 2B) and were only partially restored in cells expressing the SNARE-binding–deficient mutant Syt-1^{RK} (Figure 2B). No restoration of vesicle release probabilities was observed for the stronger loss-of-function SNARE-binding mutant Syt-1$^{RK/KK}$. Cells expressing the Syt-1^{4A} mutant, which is impaired in Ca^{2+}-stimulated membrane interactions, also exhibited release probabilities that were very low (Figure 2B). By contrast, the Syt-1^{4W} mutant, which exhibits enhanced Ca^{2+}-dependent membrane binding, was able to fully restore vesicle release probabilities (Figure 2B). The results indicated that Syt-1 regulates the probability of fu-

sion pore formation through both Ca^{2+}-dependent SNARE binding and Ca^{2+}-dependent membrane insertion. Neither Ca^{2+}-dependent Syt-1–SNARE interactions nor Ca^{2+}-dependent Syt-1-membrane interactions could compensate for the loss of the other in initiating fusion pore opening.

Syt-1 Membrane Interactions Regulate the Extent of Release from Individual Dense-Core Vesicles

To characterize the role of Syt-1–effector interactions in regulating fusion pore expansion, we examined the kinetics of individual depolarization-evoked fusion events in Syt-1/9-null cells expressing loss-of-function Syt-1[RK] or gain-of-function Syt-1[4W] mutants. ANF-GFP is a moderate-sized molecule ($\sim$6 nm) whose release by exocytosis requires expansion of a fusion pore that is initially 1–2 nm in diameter (Breckenridge and Almers, 1987; Albillos *et al.*, 1997). Individual exocytic events for ANF-EGFP, which were aligned by centering their peaks at 5 s, were characterized by a transient increase in fluorescence followed by a rapid decrease (Figure 3A). Increased fluorescence at the start of an exocytic event (at 4.25 s in Figure 3A) results from fusion pore formation and expansion with efflux of protons from the acidic dense-core vesicles (Barg *et al.*, 2002; Taraska *et al.*, 2003), which leads to enhanced EGFP fluorescence due to its pH dependence (Sawano and Miyawaki, 2000). Increases in fluorescence (to 5 s in Figure 3A) also occur as ANF-EGFP is released into the evanescent field. The ANF-EGFP quickly diffuses away from the site of release resulting in a subsequent decrease in fluorescence (5–5.75 s in Figure 3A). The majority of release events in wild-type PC12 cells terminate by cavicapture in which the fusion pore recloses with only partial release of cargo (Taraska *et al.*, 2003). For such events, the fluorescence of ANF-EGFP remaining in the vesicle undergoes a slow further decrease due to vesicle reacidification ($>$6 s in Figure 3A).

Averaged time courses for individual exocytic events with ANF-EGFP cargo did not differ significantly for wild-type cells and cells expressing Syt-1[RK] (Figure 3A). For each, the fluorescence intensity after the event (at 10 s in Figure 3A) decreased to only a small extent, which indicated incomplete ANF-EGFP release that results from fusion pore reclosure. That fusion pore reclosure and vesicle reacidification had occurred was indicated by the ability of NH_4Cl treatment, which dissipates the vesicle pH gradient, to enhance the fluorescence of exocytosed vesicles after they had dimmed (see below).

By contrast, cells expressing Syt-1[4W] exhibited marked differences from wild-type cells in the averaged time courses for individual exocytic events (Figure 3A). Most prominently, there was a greater increase in ANF-EGFP fluorescence at the peak (at 5 s) of the event (Figure 3A). This enhanced fluorescence was due to much greater ANF-EGFP release into the evanescent field because it was accompanied by larger "puffs" of fluorescence near the vesicle (Figure 3B) and was followed by a substantial postfusion reduction in fluorescence (Figure 3A at 10 s). The greater reduction in postfusion vesicle ANF-EGFP fluorescence in Syt-1[4W]–expressing cells was evident in a comparison of fluorescence loss (ΔF) values across all events in wild-type and cells expressing Syt-1[RK] or -1[4W] (Figure 3C, open vs. shaded bars).

We binned exocytic events based on decreases in fluorescence at 5 s after the peak (Figure 3C) and termed these "display," "no release" and "release" events (Figure 3, C and D). Seventeen percent of events in wild-type cells exhibited postfusion fluorescence that decreased by $>$10% compared with prefusion fluorescence (Figure 3D; termed "release").

Forty-four percent of wild-type events exhibited postfusion fluorescence that was similar to that of prefusion fluorescence ($-10\% > \Delta F > 10\%$; termed "no release"), which correspond to vesicles that exhibit very partial content release before fusion pore reclosure. Lastly, 39% of wild-type events exhibited increased fluorescence ($\Delta F < -10\%$), which were previously termed "display" events (Perrais *et al.*, 2004) that involve limited cargo release and persistent fusion pore opening. Syt-1[4W]–expressing cells exhibited a marked shift in the distribution of events by reducing "display" events (from 39 to 8%) and increasing "release" events (from 17 to 41%; Figure 3D). When we compared "release" events across cell types (Figure 3E), it was apparent that these exocytic events in cells expressing Syt-1[4W] exhibited fluorescence losses corresponding to the full release of ANF-EGFP.

The category termed "release" that exhibits fluorescence loss could include vesicles that leave the plasma membrane after exocytosis, and Syt-1[4W] might increase such events. However, we did not detect vesicle departures when we imaged exocytosing vesicles with fluorescent cargo, BDNF-EGFP, that was not released (see below). To determine whether reductions in vesicle ANF-EGFP fluorescence were accompanied by the release of ANF-EGFP, we quantified fluorescence changes using two concentric circular regions of interest, one surrounding the vesicle and the other in the surround. An increase in fluorescence in the annulus surrounding the vesicle with its subsequent decline indicated that ANF-EGFP was released and then diffused away (Figure 3, F and G; black symbols). The release of ANF-EGFP was substantially greater for cells expressing Syt-1[4W] compared with wild-type cells (Figure 3, F vs. G; black symbols). Overall, the results indicated that Syt-1[4W], a gain-of-function mutant for Ca^{2+}-dependent membrane insertion, greatly increased the release of ANF-EGFP, a cargo molecule of $\sim$6 nm, which suggests that increased fusion pore dilation occurred.
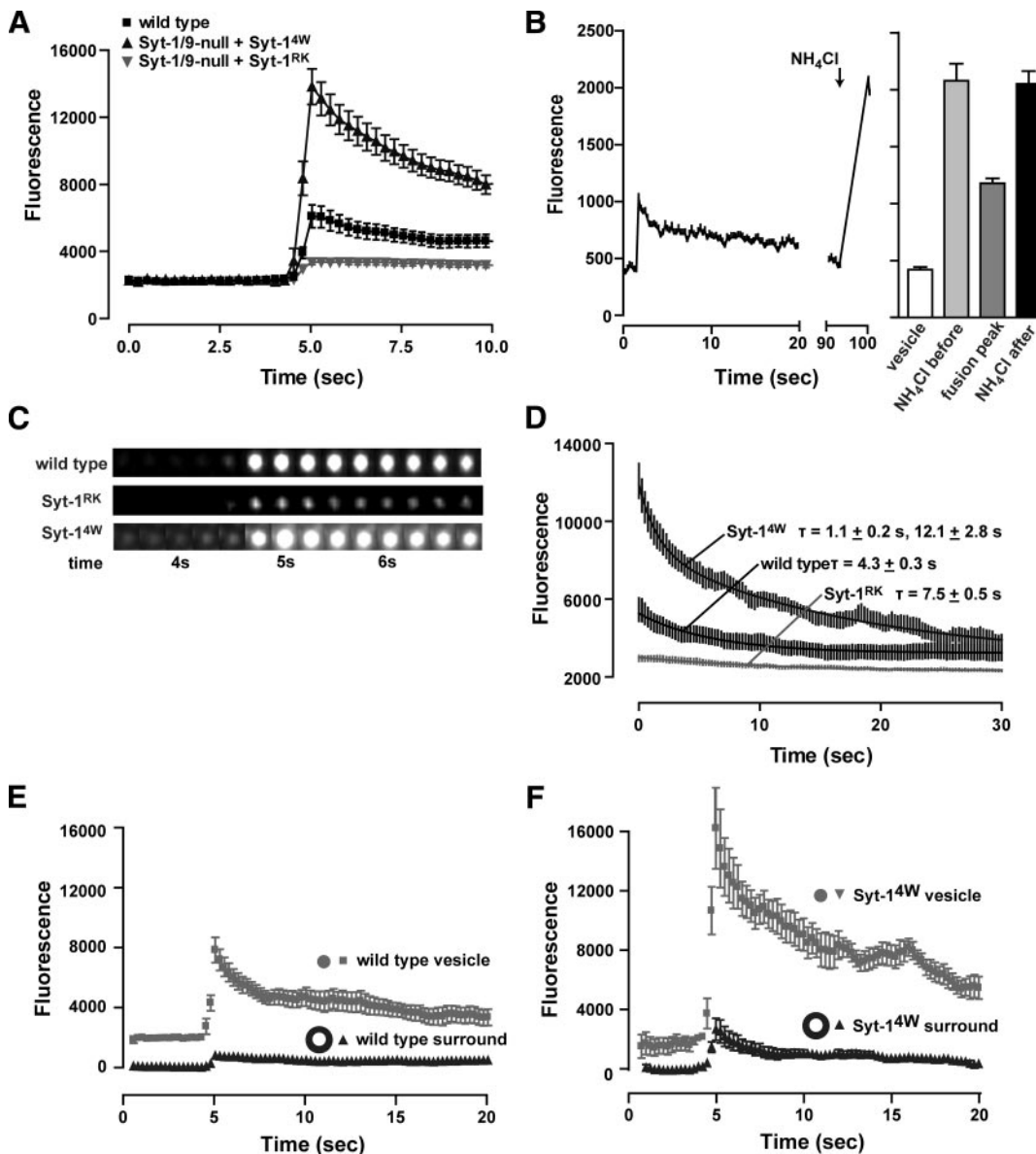
Ca^{2+}-dependent Interactions Regulate Fusion Pore Dilation

The analysis of individual exocytic events by fluorescence with ANF-EGFP cargo was complicated by its release into and diffusion out of the evanescent field. Thus, we next utilized cargo that was larger and released to a much lesser extent. A brain-derived neurotrophic factor fusion to EGFP (BDNF-EGFP) is somewhat larger than ANF-EGFP ($\sim$8 nm as a dimer) but is also strongly hindered in its release from vesicles because of condensation in the vesicle core (Brigadski *et al.*, 2005). BDNF-EGFP was uniformly packaged into dense-core vesicles independent of Syt wild-type or mutant status (Supplemental Figure S3B). We found that BDNF-EGFP was never fully released from vesicles in wild-type cells, which supported the conclusion that most exocytic events in PC12 cells terminate in cavicapture by fusion pore reclosure rather than in full fusion (Taraska *et al.*, 2003). Depolarization of wild-type cells resulted in rapid increases in BDNF-EGFP fluorescence followed by a very slow decline (Figure 4A, ■, and C). The brightening of vesicles resulted from proton efflux that was not complicated by the release of BDNF-EGFP. The subsequent very slow decline in fluorescence represented vesicle reacidification after fusion pore reclosure. This was indicated by the delayed application of NH_4Cl to dissipate proton gradients in postfusion vesicles that had fully dimmed (Figure 4B). NH_4Cl treatment increased the fluorescence of postfusion vesicles to an extent similar to that of NH_4Cl-treated prefusion vesicles, which indicated that a proton gradient had been reestablished after
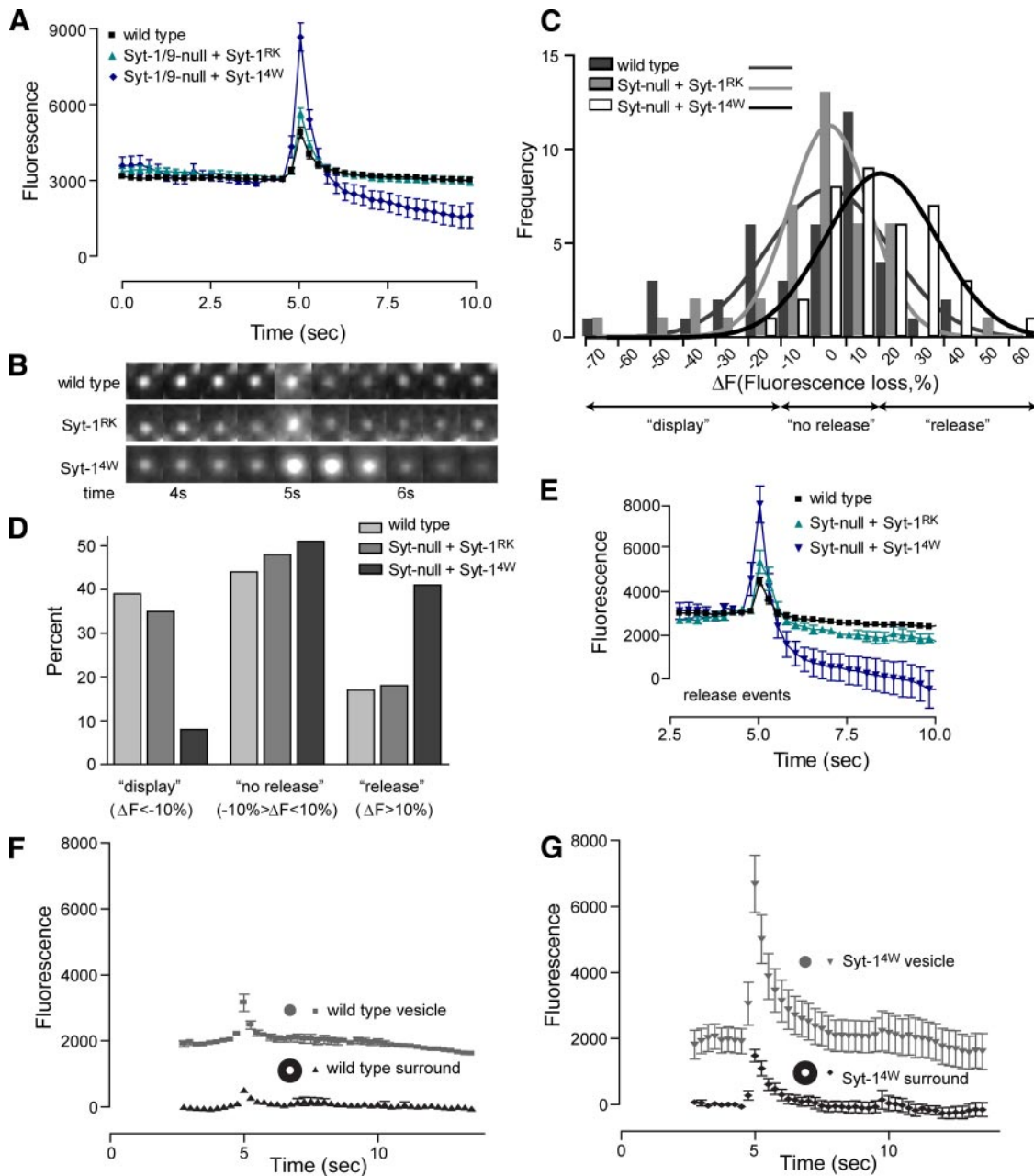
Figure 3. Syt-1[4W] drives increased ANF-EGFP cargo release. (A) Single evoked dense-core vesicle exocytic events were imaged at a time resolution of 0.25 s in cells expressing ANF-EGFP after depolarization. The average vesicle fluorescence over time was plotted for wild-type cells (n = 40), Syt-null cells expressing Syt-1[RK] (n = 40), and Syt-null cells expressing Syt-1[4W] (n = 40) by centering peak fluorescence at 5 s. Vesicle fluorescence was obtained by subtracting the background fluorescence. (B) Images of typical vesicles representing the conditions shown in A centered around 5 s are shown. (C) Distribution of vesicle fluorescence losses. The fluorescence values of ~40 exocytosed vesicles from each of the conditions shown in A was determined at t = 0 and at t = 10 s. Changes in fluorescence (ΔF) were determined by subtraction and plotted as a frequency distribution. Minus values correspond to "display" events in which fluorescence at t = 10 s exceeded that at t = 0. Positive values correspond to "release" events in which fluorescence at t = 10 s decreased relative to that at t = 0. Mean ΔF values ($\pm$SD) for wild-type (-3.9 ± 24.9) and Syt-1[RK] (-2.8 ± 21.6) did not differ, whereas those for Syt-1[4W] ($+15.1 \pm 16.8$) differed significantly (p < 0.002) from wild-type and Syt-1[RK] by a general linear model analysis of variance using the Tukey post hoc test of values. (D) The percent of exocytic events from each of the conditions shown in A (for n = 40) was determined for events in which $\Delta F < -10\%$ (display), $\Delta F = -10$–10% (no release), and $\Delta F > 10\%$. (E) The average fluorescence over time for all release events, where $\Delta F > 10\%$ was plotted for wild-type cells, Syt-null cells expressing Syt-1[RK], and Syt-null cells expressing Syt-1[4W]. Average fluorescence intensity before fusion corresponded to vesicle fluorescence with background subtracted. (F and G) The fluorescence of individual vesicle exocytic events (n = 20) from wild-type cells (F) or cells expressing Syt-1[4W] (G) were analyzed by drawing two concentric circles, one encompassing the vesicle and the other encompassing vesicle plus surround. Fluorescence in the surround (annulus) obtained by subtraction of fluorescence in outer circle from that of inner circle depicted the diffusional spread of released ANF-EGFP.

Figure 4. Syt-1–effector interactions regulate expansion of the fusion pore. (A) Single vesicle exocytic events were imaged by TIRF in cells expressing BDNF-EGFP at a time resolution of 0.25 s. The average vesicle fluorescence with time was plotted for wild-type cells (n = 40), Syt-null cells expressing Syt-1^{RK} (n = 40), and Syt-null cells expressing Syt-1^{4W} (n = 40) by centering peak fluorescence at 5 s. Average vesicle fluorescence intensity was determined by subtraction of background. (B) Dense-core vesicles reacidify after exocytosis. Left panel, the fluorescence of a representative vesicle was plotted during an exocytic event and at a later time after it had dimmed in response to 50 mM NH$_4$Cl treatment. Right panel, the fluorescence intensity (mean ±SE) of individual vesicles in cells expressing BDNF-EGFP was determined without treatment, after treatment with 50 mM NH$_4$Cl (prefusion, n = 66), with depolarization buffer to induce exocytosis (fusion, n = 65), or with depolarization buffer followed in 10 min by NH$_4$Cl treatment (postfusion, n = 38). (C) Images of typical vesicles representing the conditions shown in A centered around 5 s are shown. The diffuse fluorescence increase around Syt-1^{4W} vesicles indicated release of BDNF-EGFP. (D) The rate of the exponential decrease in fluorescence of the average individual fusion event for wild-type cells, Syt-null cells expressing Syt-1^{RK}, and Syt-null cells expressing Syt-1^{4W} was determined by fitting a one- or two-component exponential decay curve to the data shown in A. Similar τ values were obtained for experiments with 13.3-Hz recordings. (E and F) The fluorescence of individual vesicle exocytic events (n = 20) from wild-type cells (E) or cells expressing Syt-1^{4W} (F) were analyzed by drawing two concentric circles, one encompassing the vesicle and the other encompassing vesicle plus surround. Fluorescence in the surround (annulus) obtained by subtraction of fluorescence in outer circle from that of inner circle depicted the diffusional spread of released BDNF-EGFP in Syt-1^{4W}–expressing but not wild-type cells.

fusion pore reclosure. Thus, except where noted below, vesicle BDNF-EGFP served as unreleased cargo whose fluorescence increases reported proton flux out of the vesicle.

Exocytic events in cells expressing Syt-1^{RK} exhibited much smaller fluorescence increases than wild-type cells (Figure 4A, closed inverted triangles, and C). This was not due to decreased BDNF-EGFP content per vesicle in Syt-1^{RK}–expressing cells (Supplemental Figure S3B). Instead, the reduced brightening of exocytosing vesicles in Syt-1^{RK}–expressing cells appeared to be due to decreased proton efflux.

That fusion pore dilation may be limiting for proton efflux was suggested by the finding that exocytic events in wild-type cells did not brighten vesicles as fully as NH_4Cl-induced proton gradient dissipation (Figure 4B; Obermuller *et al.*, 2005). Previous studies found that proton efflux is delayed relative to fusion pore formation and requires pore dilation (Barg *et al.*, 2002). Moreover, dense-core vesicles contain substantial pH-buffering capacity, which slows the outward diffusion of protons through the pore (Wu *et al.*, 2001). Thus, the reduced brightening of vesicles in Syt-1[RK]–expressing cells (Figure 4, A and C) may indicate that fusion pore dilation was reduced or shorter in duration. These results suggested that loss-of-function in SNARE binding impairs fusion pore expansion mediated by Syt-1.

By contrast, cells expressing Syt-1[4W] exhibited fluorescence increases that were much greater than in wild-type cells (Figure 4A, ▲, and C). We interpreted this to indicate that Syt-1[4W] markedly enhanced fusion pore expansion, which allowed greater proton efflux. However, a second contribution to the increased fluorescence in Syt-1[4W] cells was from the partial release of BDNF-EGFP into the evanescent field as the result of extensive fusion pore dilation. This was indicated by three observations. First, cells expressing Syt-1[4W], but not those expressing Syt-1[RK] or wild-type, exhibited "puffs" of fluorescence near the vesicle indicating BDNF-EGFP release (Figure 4C). Second, studies of the fluorescence increases using two concentric circular regions of interest indicated that wild-type cells failed to release a diffusible puff of BDNF-EGFP (Figure 4E, ▲), whereas cells expressing Syt-1[4W] released BDNF-EGFP into the annulus surrounding the vesicle (Figure 4F, ▲). Third, an analysis of fluorescence decreases after the peak (Figure 4D), indicated that decreases for wild-type and Syt-1[RK] cells exhibited a single exponential decay ($\tau = 4.3–7.5s$) that approximated rates of vesicle reacidification (Fernandez-Alfonso and Ryan, 2006). By contrast, vesicles in Syt-1[4W] cells exhibited a two-phase exponential decay ($\tau_1 = 1.1 \pm 0.2$ s; $\tau_2 = 12.1 \pm$ 2.8 s; Figure 4D) in which the fast kinetic component likely represented diffusion of released BDNF-EGFP from sites of release. Overall, the results indicated that Syt-1[4W], a gain-of-function mutant for membrane insertion, strongly promoted fusion pore expansion that enabled release of BDNF-EGFP.

Measurement of Fusion Pore Dilation with Sized External Markers

To determine the extent of fusion pore dilation in cells expressing Syt-1[4W] and -1[RK] compared with wild-type cells, we took advantage of the finding that most exocytic events in PC12 cells terminated in cavicapture with fusion pore reclosure. Hence, a reclosed vesicle will capture external probes of different sizes based on the extent of fusion pore dilation before reclosure. We selectively monitored the capture of 10-, 40-, and 70-kDa Texas red dextrans by exocytosed vesicles that underwent cavicapture. Because exocytosed vesicles retain some BDNF-EGFP, we quantified red dextran uptake only into BDNF-EGFP–containing vesicles. In the absence of depolarizing stimulus, there was no dextran uptake into vesicles. During a 5-min incubation in depolarizing medium, an average of 22.6 ± 3.5 vesicles in wild-type cells and 24.6 ± 4.1 vesicles in Syt-1[4W]–expressing cells captured a 10-kDa dextran (~6 nm) during exocytosis (Figure 5, A and B). These numbers were similar to the number of exocytic events observed over a 5-min stimulation period, which were used to normalize the dextran uptake results (Figure 5C). The results indicated that most exocytic events in wild-type and Syt-1[4W]–expressing cells had fusion pores that expanded to a diameter of at least ~6 nm (Figure 5C). By contrast, only 3.7 ± 0.9 exocytosed vesicles captured 10-kDa dextran in cells expressing Syt-1[RK] (Figure 5, A and B). This was significantly smaller than the number of exocytic events observed for cells expressing Syt-1[RK] (Figure 5C) and indicated that not all fusion pores in these cells dilate to ~6 nm. These results showed directly
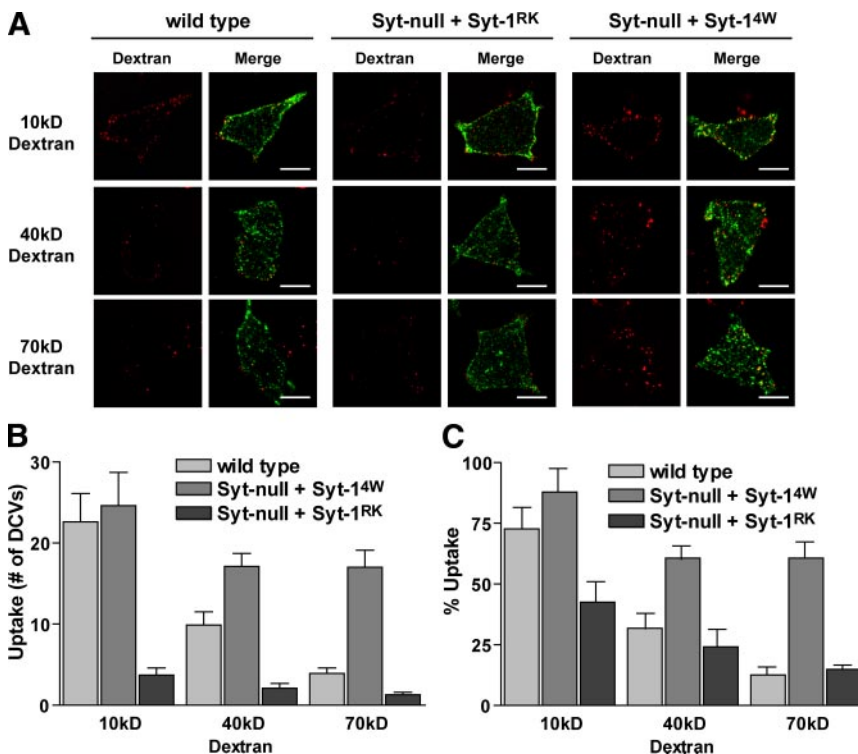
Figure 5. Syt-1-effector interactions regulate fusion pore dilation. (A) Wild-type cells, Syt-null cells expressing Syt-1[RK], and Syt-null cells expressing Syt-1[4W] that were also expressing BDNF-EGFP were incubated with dextrans (10, 40, and 70 kDa) in depolarization medium for 5 min. Representative images for the uptake of dextrans (red) into the BDNF-EGFP-containing (green) vesicles of the three cells types are shown. Scale bar, 10 μm. (B) The average number of dense-core vesicles that captured 10-, 40-, or 70-kDa dextran in a 5-min stimulation was determined for wild-type cells (n = 15 for 10 kDa, n = 35 for 40 kDa, n = 28 for 70 kDa), Syt–null cells expressing Syt-1[RK] (n = 18 for 10 kDa, n = 16 for 40 kDa, and n = 18 for 70 kDa), and Syt-null cells expressing Syt-1[4W] (n = 15 for 10 kDa, n = 20 for 40 kDa, and n = 25 for 70 kDa) and expressed as the mean ±SE. (C) The data in B were normalized to the average number of fusion events that occur in each cell type in 5 min and expressed as a percentage.

that Syt-1^{RK} with reduced Ca^{2+}-dependent SNARE binding exhibits impaired fusion pore expansion relative to wild-type cells.

In wild-type cells, only 9.9 ± 1.6 and 3.9 ± 0.7 vesicles captured 40- and 70-kDa dextrans during exocytosis, respectively (Figure 5, A and B). These results indicated that in wild-type cells only a small subset of fusion pores dilate to ~9 nm (40-kDa dextran) and an even smaller subset to ~12 nm (70-kDa dextran). By contrast, a much larger number of vesicles (17.1 ± 1.6 and 17.0 ± 2.1, respectively) captured 40- and 70-kDa dextrans in cells expressing Syt-1^{4W} (Figure 5, A–C). This indicated that the majority of fusion pores in Syt-1^{4W}–expressing cells dilate to or beyond ~12 nm (70-kDa dextran). The results showed directly that a gain-of-function Syt-1 mutant that exhibits strong Ca^{2+}-dependent membrane binding and promotes membrane curvature has a dramatic effect in promoting fusion pore expansion.

DISCUSSION

Capacitance studies revealed that elevated Ca^{2+} accelerates fusion pore expansion (Fernandez-Chacon and Alvarez de Toledo, 1995; Hartmann and Lindau, 1995), which was confirmed in amperometry studies in permeable PC12 cells, showing that Ca^{2+} reduces the lifetime of the PSF (Wang et al., 2006). That Syts regulate fusion pore expansion was suggested by the finding that Syt-1 overexpression in PC12 cells increased the lifetime of PSFs (Wang et al., 2001; Jackson and Chapman, 2006). Our studies focused on determining which Ca^{2+}-dependent properties of Syt-1 mediate its role in promoting expansion of the fusion pore. We replaced endogenous vesicle Syts in PC12 cells with defined Syt-1 point mutants and assessed the extent to which fusion pore dilation occurred in evoked exocytic events. The major conclusion from this work was that Syt-1 utilizes both Ca^{2+}-dependent SNARE interactions as well as Ca^{2+}-triggered membrane insertion to drive expansion of the fusion pore. Both of these properties of Syt-1 are also essential for Ca^{2+}-triggered fusion pore opening, which implies that the mechanisms underlying pore expansion by Ca^{2+}-bound Syt-1 are a dynamic extension of those utilized for initial pore formation. Thus, Ca^{2+}-bound Syt-1 drives a continuum of fusion pore opening followed by dilation through its interactions with SNAREs and target membrane.

The initial fusion pore for dense-core vesicles detected in capacitance studies exhibits a fluctuating conductance of ~200 pS, which is equivalent to an aqueous channel of ~1–2-nm diameter (Breckenridge and Almers, 1987; Albillos et al., 1997; Lindau and Alvarez de Toledo, 2003). Small molecules such as catecholamines experience limited release through the fusion pore, which has been detected as a PSF in amperometric recordings (Chow et al., 1992). Expansion of the pore to enable rapid further release of vesicle content has been detected by electrophysiological methods (Lindau and Alvarez de Toledo, 2003). Expansion of the pore has also been imaged by the differential release or uptake of different-sized fluorescent probes (Barg et al., 2002; Takahashi et al., 2002, 2003). In the current work, we utilized the release of ANF-EGFP, a cargo molecule of ~6 nm, or of BDNF-EGFP, a larger cargo molecule that is inefficiently released. Because of its very limited release from vesicles, BDNF-EGFP effectively served as a probe for the movement of protons, which are very small (~0.1 nm) but strongly buffered vesicle constituents. Because most dense-core vesicle exocytic events in PC12 cells occur by cavicapture, we also took advantage of the capture of external fluorescent probes to assess the extent to which fusion pore dilation occurred before reclosure.

The current work utilized Syt-1^{RK}, a Syt-1 with mutations of basic residues R199 and K200 in C2A that specifically disrupt Ca^{2+}-dependent SNARE binding without altering Syt-1 membrane interactions (Lynch et al., 2007). Cells expressing the partial loss-of-function Syt-1^{RK} exhibited strongly reduced Ca^{2+}-dependent probabilities for fusion pore opening (Figure 2B), but a sufficient number of evoked exocytic events remained to analyze the kinetics of individual events in detail. A key finding was that cells expressing Syt-1^{RK} exhibited dramatic reductions in the initial brightening of BDNF-EGFP (Figure 4A) in evoked exocytic events. Because BDNF-EGFP release did not occur, this reduction of the initial brightening of BDNF-EGFP–containing vesicles likely indicated reduced proton efflux and reduced fusion pore expansion in cells expressing Syt-1^{RK}. Some of the reduced brightening of exocytosing vesicles in Syt-1^{RK}–expressing cells may also be due to decreases in the movement of vesicles toward the plasma membrane that would accompany fuller fusion pore dilation. More direct evidence for reduced fusion pore expansion was provided by the observed reduced vesicle capture of ~6-nm dextran (Figure 5) by cells expressing Syt-1^{RK}. These observations directly implicate Ca^{2+}-dependent binding of Syt-1 to SNAREs as essential for the postfusion dilation of the fusion pore. Evidently Syt-1 interactions with membrane are inadequate to compensate for a loss in SNARE interactions. Previous studies showed that the overexpression of an inter-C2 domain linker Syt-1 mutant, which also exhibits reduced Ca^{2+}-dependent SNARE binding, failed to extend the lifetime of PSFs compared with overexpressed wild-type Syt-1 (Bai et al., 2004). Syt-1^{RK} replacement would likely extend the lifetime of PSFs because of its inability to promote fusion pore expansion but amperometry could not be utilized in the current work because of the loss in catecholamine loading into vesicles that occurs in Syt-1–deficient PC12 cells (Fukuda et al., 2002; Lynch and Martin, 2007).

We utilized Syt-1^{4W} and -1^{4A} mutants to selectively alter Ca^{2+}-dependent membrane interactions. Previous studies showed that Syt-1^{4A} retained Ca^{2+}-dependent liposome binding to a large extent but failed to induce positive membrane curvature (Martens et al., 2007). In the current work, Syt-1^{4A} exhibited reduced Ca^{2+}-dependent liposome binding (Figure 1B), but the nonequilibrium binding assay used may have emphasized the increased membrane dissociation rates that would be expected of a Syt mutant that was loosely anchored to the membrane. In any case, the reduced or enhanced activity in bilayer penetration and membrane curvature for Syt-1^{4A} and -1^{4W}, respectively, likely represent the key properties of these mutants in functional studies. The role of Syt-1 membrane interactions in determining Ca^{2+}-dependent fusion pore opening probabilities has previously been characterized. Mutation of hydrophobic residues in the Ca^{2+}-binding C2 loops 1 and 3 to tryptophan increase the Ca^{2+}-dependent probability of synaptic vesicle exocytosis (Rhee et al., 2005). The importance of Syt-1 membrane interactions for determining fusion pore opening probabilities was confirmed in the current work showing that cells expressing Syt-1^{4A} exhibited release probabilities near zero, whereas Syt-1^{4W} exhibited normal probabilities (Figure 2B). It is likely that cells expressing Syt-1^{4W} exhibited wild-type fusion probabilities, rather than enhanced probabilities reported for an Syt-1^{6W} mutant (Rhee et al., 2005), because maximal rather than graded stimulus strength was used to trigger exocytosis.

The role of Syt-1 membrane interactions in regulating fusion pore dynamics had not been previously determined. We found that the replacement of vesicle Syts with the

gain-of-function Syt-1[4W] mutant had a dramatic effect in promoting extensive fusion pore dilation. Cells with Syt-1[4W] exhibited much more release of ANF-EGFP (~6 nm; Figure 3) and, unlike wild-type cells, also released BDNF-EGFP (Figure 4). Whereas the majority of fusion pores in wild-type PC12 cells reach a diameter of 6 nm with very few dilating to 12 nm, many fusion pores in cells expressing Syt-1[4W] routinely dilated to or beyond 12 nm based on dextran-capture studies (Figure 5). In addition, there may be increased proton flux through the fusion pore in Syt-1[4W]–expressing cells compared with wild-type events based on the increased brightening of BDNF-EGFP–containing vesicles (Figure 4A). Taken together, these results indicate that the fusion pore expands to a greater diameter in cells expressing Syt-1[4W], and this is likely achieved by expansion at a greater rate. Even though full release of ANF-EGFP occurred for many vesicles in Syt-1[4W]–expressing cells (Figure 3E), full fusion was not achieved as indicated by the limited release of BDNF-EGFP (Figure 4A). Thus, it was apparent that exocytosis with extensive fusion pore dilation in Syt-1[4W]–expressing cells still terminated in cavicapture (Figure 5).

Our results with loss-of-function Syt-1[RK] and gain-of-function Syt-1[4W] mutant proteins imply important roles for both Ca²⁺-dependent SNARE binding and Ca²⁺-triggered bilayer insertion by Syt-1 in regulating fusion pore expansion. The cluster of basic residues in C2A that mediates Ca²⁺-dependent SNARE interactions is orthogonal to the membrane-penetrating loops (Lynch *et al.*, 2007), which would enable simultaneous interactions of Syt-1 with SNAREs and the target membrane, which has been shown in studies in vitro (Davis *et al.*, 1999; Dai *et al.*, 2007). Both interactions appear to function to promote fusion pore expansion but the exact mechanisms utilized are uncertain.

The composition of the fusion pore, whether lipidic or protein-lined or both, remains to be determined (Chernomordik *et al.*, 2006). Recent studies suggested that trans-membrane segments of syntaxin-1 line the fusion pore on the plasma membrane (Han *et al.*, 2004). Continued Syt-1 interactions with SNAREs beyond initial fusion pore formation might drive the lateral separation of SNARE complexes to expand the pore. Syt-1 penetration of the plasma membrane by the tandem C2 domains would induce positive membrane curvature, possibly within a ring of SNARE complexes, to lower the activation barrier for bilayer fusion in opening of the fusion pore (Martens *et al.*, 2007). The lateral tension of the curved plasma membrane bilayer would be expected to drive further expansion of the fusion pore (Chernomordik and Kozlov, 2005). Although higher resolution studies will be required to define the underlying mechanisms, the current work indicates that both SNAREs as well as membrane tension participate in pore expansion and its regulation by Syt-1.

ACKNOWLEDGMENTS

REFERENCES

Albillos, A., Dernick, G., Horstmann, H., Almers, W., Alvarez de Toledo, G., and Lindau, M. (1997). The exocytotic event in chromaffin cells revealed by patch amperometry. Nature *389*, 509–512.

Alvarez de Toledo, G., Fernandez-Chacon, R., and Fernandez, J. M. (1993). Release of secretory products during transient vesicle fusion. Nature *363*, 554–558.

Bai, J., and Chapman, E. R. (2004). The C2 domains of synaptotagmin—partners in exocytosis. Trends Biochem. Sci. *29*, 143–151.

Bai, J., Wang, C. T., Richards, D. A., Jackson, M. B., and Chapman, E. R. (2004). Fusion pore dynamics are regulated by synaptotagmin*t-SNARE interactions. Neuron *41*, 929–942.

Bai, J., Wang, P., and Chapman, E. R. (2002). C2A activates a cryptic Ca²⁺-triggered membrane penetration activity within the C2B domain of synaptotagmin I. Proc. Natl. Acad. Sci. USA *99*, 1665–1670.

Barg, S., Olofsson, C. S., Schreiver-Abeln, J., Wendt, A., Gebre-Medhin, S., Renstrom, E., and Rorsman, P. (2002). Delay between fusion pore opening and peptide release from large dense-core vesicles in neuroendocrine cells. Neuron *33*, 287–299.

Bhalla, A., Chicka, M. C., Tucker, W. C., and Chapman, E. R. (2006). Ca²⁺-synaptotagmin directly regulates t-SNARE function during reconstituted membrane fusion. Nat. Struct. Mol. Biol. *13*, 323–330.

Breckenridge, L. J., and Almers, W. (1987). Currents through the fusion pore that forms during exocytosis of a secretory vesicle. Nature *328*, 814–817.

Brigadski, T., Hartmann, M., and Lessmann, V. (2005). Differential vesicular targeting and time course of synaptic secretion of the mammalian neurotrophins. J. Neurosci. *25*, 7601–7614.

Chapman, E. R. (2002). Synaptotagmin: a Ca²⁺ sensor that triggers exocytosis? Nat. Rev. Mol. Cell Biol. *3*, 498–508.

Chernomordik, L. V., and Kozlov, M. M. (2005). Membrane hemifusion: crossing a chasm in two leaps. Cell *123*, 375–382.

Chernomordik, L. V., Zimmerberg, J., and Kozlov, M. M. (2006). Membranes of the world unite! J. Cell Biol. *175*, 201–207.

Chow, R. H., von Ruden, L., and Neher, E. (1992). Delay in vesicle fusion revealed by electrochemical monitoring of single secretory events in adrenal chromaffin cells. Nature *356*, 60–63.

Cohen, F. S., and Melikyan, G. B. (2004). The energetics of membrane fusion from binding, through hemifusion, pore formation, and pore enlargement. J. Membr. Biol. *199*, 1–14.

Craxton, M. (2007). Evolutionary genomics of plant genes encoding N-terminal-TM-C2 domain proteins and the similar FAM62 genes and synaptotagmin genes of metazoans. BMC Genomics *8*, 259.

Dai, H., Shen, N., Arac, D., and Rizo, J. (2007). A quaternary SNARE-synaptotagmin-Ca²⁺-phospholipid complex in neurotransmitter release. J. Mol. Biol. *367*, 848–863.

Davis, A. F., Bai, J., Fasshauer, D., Wolowick, M. J., Lewis, J. L., and Chapman, E. R. (1999). Kinetics of synaptotagmin responses to Ca²⁺ and assembly with the core SNARE complex onto membranes. Neuron *24*, 363–376.

Earles, C. A., Bai, J., Wang, P., and Chapman, E. R. (2001). The tandem C2 domains of synaptotagmin contain redundant Ca²⁺ binding sites that cooperate to engage t-SNAREs and trigger exocytosis. J. Cell Biol. *154*, 1117–1123.

Fernandez-Alfonso, T., and Ryan, T. A. (2006). The efficiency of the synaptic vesicle cycle at central nervous system synapses. Trends Cell Biol. *16*, 413–420.

Fernandez-Chacon, R., and Alvarez de Toledo, G. (1995). Cytosolic calcium facilitates release of secretory products after exocytotic vesicle fusion. FEBS Lett. *363*, 221–225.

Fukuda, M., Kanno, E., Satoh, M., Saegusa, C., and Yamamoto, A. (2004). Synaptotagmin VII is targeted to dense-core vesicles and regulates their Ca²⁺-dependent exocytosis in PC12 cells. J. Biol. Chem. *279*, 52677–52684.

Fukuda, M., Kowalchyk, J. A., Zhang, X., Martin, T. F., and Mikoshiba, K. (2002). Synaptotagmin IX regulates Ca²⁺-dependent secretion in PC12 cells. J. Biol. Chem. *277*, 4601–4604.

Geppert, M., Goda, Y., Hammer, R. E., Li, C., Rosahl, T. W., Stevens, C. F., and Sudhof, T. C. (1994). Synaptotagmin I: a major Ca²⁺ sensor for transmitter release at a central synapse. Cell *79*, 717–727.

Gerona, R. R., Larsen, E. C., Kowalchyk, J. A., and Martin, T. F. (2000). The C terminus of SNAP25 is essential for Ca²⁺-dependent binding of synaptotagmin to SNARE complexes. J. Biol. Chem. *275*, 6328–6336.

Granath, K. A., and Kvist, B. E. (1967). Molecular weight distribution analysis by gel chromatography on Sephadex. J. Chromatograph. *28*, 69–81.

Gustavsson, N., Lao, Y., Maximov, A., Chuang, J. C., Kostromina, E., Repa, J. J., Li, C., Radda, G. K., Sudhof, T. C., and Han, W. (2008). Impaired insulin secretion and glucose intolerance in synaptotagmin-7 null mutant mice. Proc. Natl. Acad. Sci. USA *105*, 3992–3997.

Han, X., Wang, C. T., Bai, J., Chapman, E. R., and Jackson, M. B. (2004). Transmembrane segments of syntaxin line the fusion pore of Ca^{2+}-triggered exocytosis. Science 304, 289–292.

Hartmann, J., and Lindau, M. (1995). A novel Ca^{2+}-dependent step in exocytosis subsequent to vesicle fusion. FEBS Lett. 363, 217–220.

Henkel, A. W., and Almers, W. (1996). Fast steps in exocytosis and endocytosis studied by capacitance measurements in endocrine cells. Curr. Opin. Neurobiol. 6, 350–357.

Herrick, D. Z., Sterbling, S., Rasch, K. A., Hinderliter, A., and Cafiso, D. S. (2006). Position of synaptotagmin I at the membrane interface: cooperative interactions of tandem C2 domains. Biochemistry 45, 9668–9674.

Iezzi, M., Eliasson, L., Fukuda, M., and Wollheim, C. B. (2005). Adenovirus-mediated silencing of synaptotagmin 9 inhibits Ca^{2+}-dependent insulin secretion in islets. FEBS Lett. 579, 5241–5246.

Jackson, M. B., and Chapman, E. R. (2006). Fusion pores and fusion machines in Ca2+-triggered exocytosis. Annu. Rev. Biophys. Biomol. Struct. 35, 135–160.

Lindau, M., and Alvarez de Toledo, G. (2003). The fusion pore. Biochim. Biophys. Acta 1641, 167–173.

Lynch, K. L., Gerona, R. R., Larsen, E. C., Marcia, R. F., Mitchell, J. C., and Martin, T. F. (2007). Synaptotagmin C2A loop 2 mediates Ca^{2+}-dependent SNARE interactions essential for Ca^{2+}-triggered vesicle exocytosis. Mol. Biol. Cell 18, 4957–4968.

Lynch, K. L., and Martin, T. F. (2007). Synaptotagmins I and IX function redundantly in regulated exocytosis but not endocytosis in PC12 cells. J. Cell Sci. 120, 617–627.

Martens, S., Kozlov, M. M., and McMahon, H. T. (2007). How synaptotagmin promotes membrane fusion. Science 316, 1205–1208.

Obermuller, S., Lindqvist, A., Karanauskaite, J., Galvanovskis, J., Rorsman, P., and Barg, S. (2005). Selective nucleotide-release from dense-core granules in insulin-secreting cells. J. Cell Sci. 118, 4271–4282.

Paddison, P. J., Caudy, A. A., Bernstein, E., Hannon, G. J., and Conklin, D. S. (2002). Short hairpin RNAs (shRNAs) induce sequence-specific silencing in mammalian cells. Genes Dev. 16, 948–958.

Pang, Z. P., Shin, O. H., Meyer, A. C., Rosenmund, C., and Sudhof, T. C. (2006). A gain-of-function mutation in synaptotagmin-1 reveals a critical role of Ca^{2+}-dependent soluble N-ethylmaleimide-sensitive factor attachment protein receptor complex binding in synaptic exocytosis. J. Neurosci. 26, 12556–12565.

Perrais, D., Kleppe, I. C., Taraska, J. W., and Almers, W. (2004). Recapture after exocytosis causes differential retention of protein in granules of bovine chromaffin cells. J. Physiol. 560, 413–428.

Rhee, J. S., Li, L. Y., Shin, O. H., Rah, J. C., Rizo, J., Sudhof, T. C., and Rosenmund, C. (2005). Augmenting neurotransmitter release by enhancing the apparent Ca^{2+} affinity of synaptotagmin 1. Proc. Natl. Acad. Sci. USA 102, 18664–18669.

Rizo, J., Chen, X., and Arac, D. (2006). Unraveling the mechanisms of synaptotagmin and SNARE function in neurotransmitter release. Trends Cell Biol. 16, 339–350.

Rizo, J., and Sudhof, T. C. (1998). C2-domains, structure and function of a universal Ca^{2+}-binding domain. J. Biol. Chem. 273, 15879–15882.

Sawano, A., and Miyawaki, A. (2000). Directed evolution of green fluorescent protein by a new versatile PCR strategy for site-directed and semi-random mutagenesis. Nucleic Acids Res. 28, e78.

Schoenmakers, T. J., Visser, G. J., Flik, G., and Theuvenet, A. P. (1992). CHELATOR: an improved method for computing metal ion concentrations in physiological solutions. Biotechniques 12, 870–879.

Schonn, J. S., Maximov, A., Lao, Y., Sudhof, T. C., and Sorensen, J. B. (2008). Synaptotagmin-1 and -7 are functionally overlapping Ca^{2+} sensors for exocytosis in adrenal chromaffin cells. Proc. Natl. Acad. Sci. USA 105, 3998–4003.

Sudhof, T. C. (2004). The synaptic vesicle cycle. Annu. Rev. Neurosci. 27, 509–547.

Sun, J., Pang, Z. P., Qin, D., Fahim, A. T., Adachi, R., and Sudhof, T. C. (2007). A dual-Ca^{2+}-sensor model for neurotransmitter release in a central synapse. Nature 450, 676–682.

Takahashi, N., Kishimoto, T., Nemoto, T., Kadowaki, T., and Kasai, H. (2002). Fusion pore dynamics and insulin granule exocytosis in the pancreatic islet. Science 297, 1349–1352.

Taraska, J. W., Perrais, D., Ohara-Imaizumi, M., Nagamatsu, S., and Almers, W. (2003). Secretory granules are recaptured largely intact after stimulated exocytosis in cultured endocrine cells. Proc. Natl. Acad. Sci. USA 100, 2070–2075.

Tucker, W. C., Edwardson, J. M., Bai, J., Kim, H. J., Martin, T. F., and Chapman, E. R. (2003). Identification of synaptotagmin effectors via acute inhibition of secretion from cracked PC12 cells. J. Cell Biol. 162, 199–209.

Wang, C. T., Bai, J., Chang, P. Y., Chapman, E. R., and Jackson, M. B. (2006). Synaptotagmin-Ca^{2+} triggers two sequential steps in regulated exocytosis in rat PC12 cells: fusion pore opening and fusion pore dilation. J. Physiol. 570, 295–307.

Wang, C. T., Grishanin, R., Earles, C. A., Chang, P. Y., Martin, T. F., Chapman, E. R., and Jackson, M. B. (2001). Synaptotagmin modulation of fusion pore kinetics in regulated exocytosis of dense-core vesicles. Science 294, 1111–1115.

Wang, C. T., Lu, J. C., Bai, J., Chang, P. Y., Martin, T. F., Chapman, E. R., and Jackson, M. B. (2003). Different domains of synaptotagmin control the choice between kiss-and-run and full fusion. Nature 424, 943–947.

Wang, P., Chicka, M. C., Bhalla, A., Richards, D. A., and Chapman, E. R. (2005). Synaptotagmin VII is targeted to secretory organelles in PC12 cells, where it functions as a high-affinity calcium sensor. Mol. Cell. Biol. 25, 8693–8702.

Weber, T., Zemelman, B. V., McNew, J. A., Westermann, B., Gmachl, M., Parlati, F., Sollner, T. H., and Rothman, J. E. (1998). SNAREpins: minimal machinery for membrane fusion. Cell 92, 759–772.

Wu, M. M., Grabe, M., Adams, S., Tsien, R. Y., Moore, H. P., and Machen, T. E. (2001). Mechanisms of pH regulation in the regulated secretory pathway. J. Biol. Chem. 276, 33027–33035.

Xiong, X., Zhou, K. M., Wu, Z. X., and Xu, T. (2006). Silence of synaptotagmin I in INS-1 cells inhibits fast exocytosis and fast endocytosis. Biochem. Biophys. Res. Commun. 347, 76–82.

Xu, J., Mashimo, T., and Sudhof, T. C. (2007). Synaptotagmin-1, -2, and-9, Ca^{2+} sensors for fast release that specify distinct presynaptic properties in subsets of neurons. Neuron 54, 567–581.

Zhang, X., Kim-Miller, M. J., Fukuda, M., Kowalchyk, J. A., and Martin, T. F. (2002). Ca^{2+}-dependent synaptotagmin binding to SNAP-25 is essential for Ca^{2+}-triggered exocytosis. Neuron 34, 599–611.

Zhang, X., Rizo, J., and Sudhof, T. C. (1998). Mechanism of phospholipid binding by the C2A-domain of synaptotagmin I. Biochemistry 37, 12395–12403.
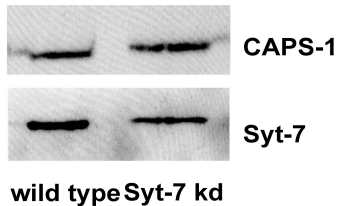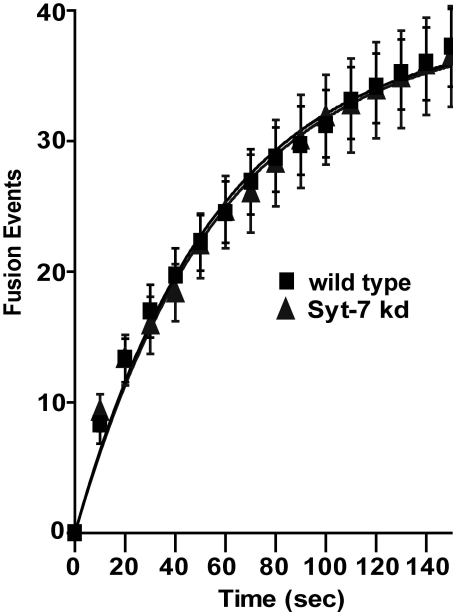
Supplemental Fig. 1. Knock down of Syt-7 does not affect evoked dense-core vesicle exocytosis in PC12 cells. Exocytic events were monitored as changes in ANF-EGFP fluorescence in 10s intervals and plotted cumulatively in wild-type cells and cells transfected with a Syt-7-directed shRNA plasmid. Western blotting and densitometry indicated that the Syt-7 shRNA plasmid reduced Syt-7 levels by at least 60%. CAPS-1 is shown as a loading control.
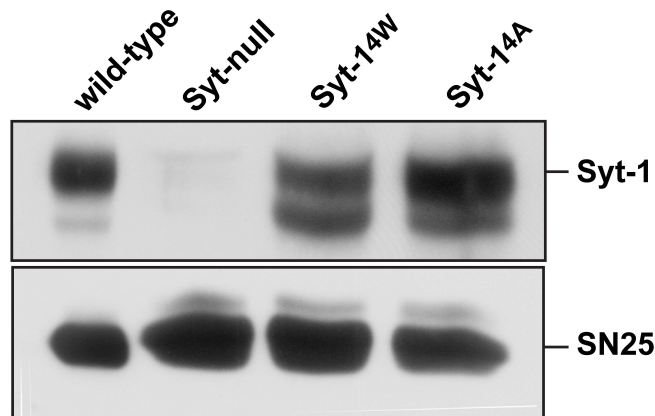
Supplemental Fig. 2. Syt-1^{4A} and Syt-1^{4W} are re-expressed and appropriately targeted to dense-core vesicles in Syt-1/9-null PC12 cells. **(A)** Western blotting was used to compare Syt-1 levels in wild-type cells and Syt-1/9-null cells versus null cells re-expressing Syt-1^{4W} or Syt-1^{4A}. 10 μg of cell lysate was analyzed per lane with immunoblotted SNAP-25 as a loading control. **(B)** Immunocytochemistry with Syt-1 antibody was used to localize Syt-1^{4W} and Syt-1^{4A} re-expressed in Syt-null PC12 cells. The re-expressed proteins exhibited a punctate distribution resembling that of chromogranin B (CgB), a dense-core vesicle protein. The Syt-1 antibody exhibited a degree of non-specific staining evident in the Syt-null cells that did not co-localize with CgB.

Supplemental Fig. 3. **(A)** ANF-EGFP is expressed and targeted to dense-core vesicles similarly in wild-type or Syt-1 mutant-expressing cells. Distribution shows the vesicle ANF-EGFP fluorescence (background subtracted) for 150 vesicles determined by TIRF microscopy in wild-type, Syt-1^{RK}-expressing or Syt-1^{4W}-expressing cells. Mean (± SE) fluorescence values were 3093 ± 182 for wild-type, 2699 ± 168 for Syt-1^{RK}, and 3025 ± 173 for Syt-1^{4W}, which were not significantly different. **(B)** BDNF-EGFP is expressed and targeted to dense-core vesicles similarly in wild-type or Syt-1 mutant-expressing cells. Distribution shows the vesicle BDNF-EGFP fluorescence (background subtracted) for 100 vesicles determined by TIRF microscopy in wild-type, Syt-1^{RK}-expressing or Syt-1^{4W}-expressing cells. Mean (± SE) fluorescence values were 2063 ± 163 for wild-type, 2106 ± 176 for Syt-1^{RK}, and 2417 ± 178 for Syt-1^{4W}, which were not significantly different. **(C)** Syt-1 mutants do not affect the number of plasma membrane-proximal vesicles. Dense-core vesicles containing ANF-EGFP were counted in cell footprints by TIRF microscopy and

normalized to calculated footprint area (mean ± SE). Wild-type cells (n=20) did not differ significantly from Syt-1/9-null cells that expressed Syt-1^{RK} (n=18), Syt-1$^{RK/KK}$ (n=15), Syt-1^{4A} (n=10) or Syt-1^{4W} (n=10) mutants.

A

| wild-type | Syt-null | Syt-14W | Syt-14A |

Syt-1

SN25

B

Syt-1 pAb CgB mAb Merge

Syt-1/9-null +Syt-14W

Syt-1/9-null +Syt-14A

Syt-1/9-null